Metallurgical and Materials Engineering *Research Paper*
Association of Metallurgical Engineers of Serbia AMES *https://doi.org/10.30544/725*

NUMERICAL INVESTIGATION OF THE NANOPARTICLES NATURE EFFECT ON THE MHD BEHAVIOR IN A SQUARE CAVITY WITH A METALLIC OBSTACLE

Fayçal Bouzit[1], Mohamed Bouzit[1], Abderrahim Mokhefi[2]*

[1]Laboratory of Marine Sciences and Engineering (LSIM), Faculty of Mechanical Engineering,Université des Sciences et de la Technologie Mohammed Boudiaf USTOMB, B.P.1505, El M'naouer. Oran, Algérie
[2]Mechanics, Modeling and Experimentation Laboratory L2ME, Faculty of Sciences and Technology, Bechar University B.P.417, 08000, Bechar, Algeria

Received 31.08.2022
Accepted 03.11.2022

Abstract

In this paper, a study is conducted to determine numerically the effect of the nanoparticles nature (Al_2O_3, CuO, and Fe_3O_4) on the thermo-magnetohydrodynamic behavior of a nanofluid in a square cavity with a circular obstacle. The left wall of this cavity is movable and provided with a cold temperature (Tc) and the right wall is exposed to a hot temperature (Th). However, the upper and lower walls are considered adiabatic. The purpose of this paper is to highlight the effect of aluminum dioxide, copper oxide, and iron trioxide nanoparticles on the thermal and hydrodynamic behavior under the influence of different volume fractions($0 \leq \varphi \leq 0.1$), different Hartmann numbers ($0 \leq Ha \leq 75$) and Richardson number ($0 \leq Ri \leq 5$). The system of governing équations was solved by the finite element method adopting the Galerkine discretization. The obtained results showed that the CuO nanoparticles improve the heat transfer at the fluid and obstacle, in addition, the increase of Hartmann number reduces the heat capacity, especially with the use of Fe3O4 nanoparticles. This study falls within the context of improving the cooling rate of industrial equipment.

Keywords: Nanoparticles; thermo-magnetohydrodynamic; Al_2O_3; CuO and Fe_3O_4; finite element method.

1. Introduction

The free convection phenomenon inside lid-driven cavity has a sensitive impact on a variety of engineering applications such as atmospheric flow, lubrification and drying technologies, food industry, and cooling of electronic components. In this

[*]Corresponding author: Abderrahim Mokhefi, *abderahimmokhefi@yahoo.fr*

respect, the study of the natural convection phenomenon inside lid-driven cavities was of a great interest from many researchers in such field.

The application of heat exchangers based on natural convection is the most implemented, due to the moderation of the dissipation of energy, operating noise, and the high consistency of mechanical equipment compared to those involving fluid circulation by forced convection. However, the low thermal conductivity of conventional heat transfer fluids presents an impediment to the performance of these natural systems.

Magnetohydrodynamic (MHD) natural convection in the presence of nanofluids, is an important scientific branch for several applications in engineering fields such as crystal growth, liquid metal, microelectronic devices, etc. It aims to utilize the natural convection advantages of the high thermal conductivity of nanofluids filled in enclosures and subjected to external magnetic fields.

Numerical analysis of the combined effect of MHD mixed convection and Joule heating of an electrically conductive fluid in a lidded cavity with a heated source was performed by *Rahman et al.* [1]. The computational results are presented and discussed for values of Ri =0 to 5, Ha=0 to 50, and J=0 to 7.5 and indicate that the parameters Ha and J affect the heat transfer, temperature distributions, and flow fields in the cavity. They indicate that the parameters Ha and J affect the heat transfer, temperature distributions, and flow fields in the cavity. They also found that the magnetic field has a marked influence on heat transfer and fluid flow. *Mahmoudi et al.* [2] investigate the entropy generation and enhancement of heat transfer by natural convectionusing Cu–water nanofluid in the presence of a constant magneticfield inside a trapezoidal enclosure. They have shown that the enhancement of the Nusselt number dueto the presence of nanoparticles increases with the Hartman number at the middle Rayleigh number. On the other hand, they haveobserved a reduction in heat transfer at a higher Rayleigh number. *Bourantas et al.* [3] have considered a transient laminar natural-convection flow of a micropolar-nanofluid Al_2O_3-water in the presence of amagnetic field in an inclined rectangular enclosure. In this work, it has been demonstrated that the local Nusselt number increases considerably with the effect of buoyancy since the circulation becomes stronger. On the other hand, a significant reduction in the local Nusselt number due to the effect of the magneticfield is observed.

the Lattice-Boltzmann method was used by *Mahmoudi et al.* [4] to examine the natural convection in a square enclosure subjectedtoamagnetic field and filled with a water-Al_2O_3 nanofluid. Their results have shown that the heat transfer rate increases with the buoyancy effect but it decreases with an increase of the magnetic field intensity. *Ghaffarpas et al.* [5] carried out a numerical study by the use of thefinite volume method ofthe magnetohydrodynamic natural convection inside a sinusoidally heated lid-driven cavity filled with Fe_3O_4 -water nanofluid where the effect of Joule heating has been considered. He observed that, in the presence of Joule heating, the addition of ferrite nanoparticles to the base fluid enhance the rate of heat transfer. In the study of *Yousofvand et al.* [6], they have performed the Lattice-Boltzmann method to analyze the MHD mixed convection inside an electromagnetic pump, in the presence of Cu-water nanofluid. Their numerical results have indicated the existence of an optimum magnetic intensity showing a positive effect of the buoyancy and the electric field parameter on the Nusselt number. *Aghamajidia et al.* [7] utilized the Tiwari-Das model

to studythe natural-convective flow of an electrically conducting nanofluid adjacent to a spinning down-pointing vertical one in the presence of a transverse magnetic field. Their simulation represents the feasibility of using magnetic rotating body drives in novel nuclear space propulsion engines and this model has important applications in heat transfer enhancement in renewable energy systems and industrial thermal management. The work of *Ahmed et al.* [8] is a numerical simulation of magnetohydrodynamic natural convection and heat transfer of nanofluids flow inside wavy enclosures filled with a heat-generating porous medium has been carried out using Buongiorno's model, they found that the heat transfer rate is an increasing function in both the undulation number and the wavy contraction ratio. Mkhatshwa et al. [9] investigated the magnetohydrodynamic flow, heat, and mass transfer characteristics ina silver water nanofluid about a vertical slender cylinder by considering diffusion-thermal,thermo-diffusion, chemical reaction, and Hall effects, they found that the introduction of chemically reactive species, nanoparticle volume fraction and Soret effect leads to enhancementof the mass transfer characteristics.

Ghasemi et al. [10] have given an investigation of the mixed MHD convection of the Cu-water nanofluid flow inside a three-dimensional enclosure with lid-driven walls. They have developed the multi-relaxation time lattice Boltzmann method code to solve the governing equations, they have shown that the transverse and opposed mixed convection modes have significant negative effects on the heat transfer. *Mliki et al.* [11] studied the entropy generation of MHD natural convectionheat transfer in a heated incinerator,in the presence of (Al_2O_3-Cu/H_2O) hybrid-nanofluid and using the lattice Boltzmann method, their numerical results demonstrated that in the case of considering the conductive heat transfer regime theeffect of Lorentz force is reduced. The influence of opposing thermal buoyancy on heat transfer and fluid flow through a 180° curved square section channel was treated by *Bouzit et al.* [12,19] for values (Re = 40 to 1000, Ri = -1 to 0 and 0 to 1 and n = 0.4 to 1.2). Thier results showed that an additional longitudinal vorticeshave been formed on the ductwalls. On the other hand, they have shown that the size and the number of these vortices increase progressively with increasing Reynolds number, Richardson number, and power-law index. They have also found that the Richardson number and Reynolds number increase the heat transfer rate.

Mahanthesh et al. [14] studied the two-phase hydromagnetic flow of a viscous fluid through a suspension of dust and nanoparticles. They have taken into consideration the impact of Hall current and the characterization of various nanoparticles type (Cu, Al2O3, TiO2, and Ag) on the velocity and temperature profiles. Animasaun et al. [15] have discussed under the influence of a magnetic field, the boundary layer flow of two nanofluids Al2O3-water with differents Al2O3 nanoparticle diameters on a surface of a paraboloid of revolution. They have found that the magnetic field has dual effects on the transverse flow profiles in the case of the two nanofluids.

Mahanthesh et al. [13] treated the transient of the two-phase boundary layer flow of a dusty (TiO2-EO) nanofluid on the temperature profile with the impacts of Hall current, nonlinear radiative heat, and an irregular heat source. In the same aspect, Mahanthesh et al. [17] examined in the presence of a strong magnetic field, the two-phase flow of an electrically conductive fluid over a permeable stretching sheet. They have shown that the influence of injection and suction are opposite on the growth of the momentum boundary layer.

Gireesha et al. [16-18] have studied the different physical aspects of dust where a nanofluid flows in the boundary layer. They have highlighted the effects of the Hall current, the Darcy porous medium and the thermal radiation on the thermal state. They have demonstrated that the Hall current has a significant influence on the hydrodynamic and the thermal fields. A numerical study carried out by *A.Mokhefi et al* [25-27] on the thermal and hydrodynamic effect of the non-isothermal laminar flow of an Al_2O_3-water nanofluid in a mechanically agitated tank using the finite element method. The obtained results showed that the addition of Al_2O_3 in the fluid improves the heat transfer in the tank, It was also noted that the stirring power increases with the volume fraction of alumina nanoparticles. This study was followed by [27] using a wavy wall of a stirred tank with a flat bottom equipped with an anchor stirrer, the results of this numerical simulation showed a considerable acceleration of heat transfer inside the stirred tank by increasing the amplitude of the wavy wall and increasing the concentration of nanoparticles. Still, with Al_2O_3/water nanofluid, a numerical study made by *Bourantas et al*. [26] of natural convection of a micropolar nanofluid (Al_2O_3/water) in a tilted rectangular enclosure in the presence of a magnetic field, several parameters were varied, such as Hartman (Ha), Rayleigh (Ra) numbers, volume fractions (u), tilt angle and magnetic field directions. Their results show that the magnetic field orientation and intensity significantly affect the flow and temperature fields. An analysis of the stable natural MHD convection was done by *Mejri et al.* [28] using the LBM method to generate the entropy of the Al_2O_3-water nanofluid in a square chamber, they found that the addition of nanoparticles does not affect the entropy generation, but, it increases the heat transfer.

Ali et al. [32] studied analytically and graphically the flow of water-based fractional nanofluid on a vertical plate moving with a heat source. They found that the fractional parameters have a remarkable influence on the heat transfer and the fluid movement, this transfer is more important for the fractional nanofluid compared to the ordinary nanofluid. The heat transfer analysis of fractional nanofluids containing Cu, CuO, and Ag as nanoparticles on an infinite vertical plate under the influence of temperature and thermal radiation has been treated by *Madhura et al.*[33], the results indicate that the fractional parameter and the volume fraction of nanoparticles have an impact on the different parameters related to the flow.Narahari et al [34] investigated analytically the transient free convection flow of nanofluids between two long parallel vertical plates in the presence of thermal radiation. The effect of the nature of the water-based nanofluids (Cu, Ag, CuO, TiO_2, and Al_2O_3), the volume fraction of the nanoparticles, the radiation parameter and the time variable on the velocity, temperature, skin friction, Nusselt number, volume flow rate and vertical heat flux were discussed.Heat and mass transfer of two-phase MHD dusty nanofluids on a vertical wavy sinusoidal surface is studied by *Kalpana et al.* [35], the effects of Brownian motion, thermophoresis, and the nature of the nanofluid (Al_2O_3-water, Cu-water, TiO_2-water) immersed in conductive dust particles were considered, they compared their results of the coefficient of skin friction, heat and mass transfer rate to the literature.

Based on these studies on the heat transfer of a nanofluid in a square cavity, we notice the lack of studies on the influence of the nanofluid nature on the MHD behavior in a square cavity. Consequently, this paper aims to give a fine knowledge of the effect of the metallic nature of nanoparticles (Al_2O_3, CuO, and Fe_3O_4) on the thermo-

magnetohydrodynamic behavior of a nanofluid in a square cavity equipped with a circular obstacle.

The present problem considers the effect of the magnetic field on the evolution of heat transfer. This type of problem is often encountered in electronic cooling equipment such as CPU coolers, where the flow undergoes magnetic field lines leakage from neighboring equipment.

The effect of the volume fraction, the Hartmann number, and the Richardson number on the heat transfer in the cavity has been highlighted. The obtained results are presented and discussed for the range of these parameters as follows: Re = 100, J = 0, Pr = 0.71, φ = 0 to 0.1, Ha = 0 to 75and Ri = 0 to 5.

2. Mathematical formulation

Thetwo-dimensionallaminar flow is generated by mixed convection in the computational domainillustrated inFigure.1. The model considered is a square cavity with length sides *L*. The upper and lower walls of the cavity are assumed to be adiabatic. The left vertical wall is maintained at a cold temperature T_c, and can move in its own plane at a constant velocity U_0, while the right vertical wall is maintained at a hot temperature T_h. The cavity walls are assumed to be electrically insulating and the fluid is assumedto be electrically conductive.In the center of the cavity, there is a circular metallic obstacle ofdiameter *d* and a non-slip wall. A thermal continuity has been imposed at the interface between this obstacle and the nanofluid. The cavity-obstacle system is subject to a horizontal magnetic field B_0whose force of Lorentz acts in the vertical downwarddirection.

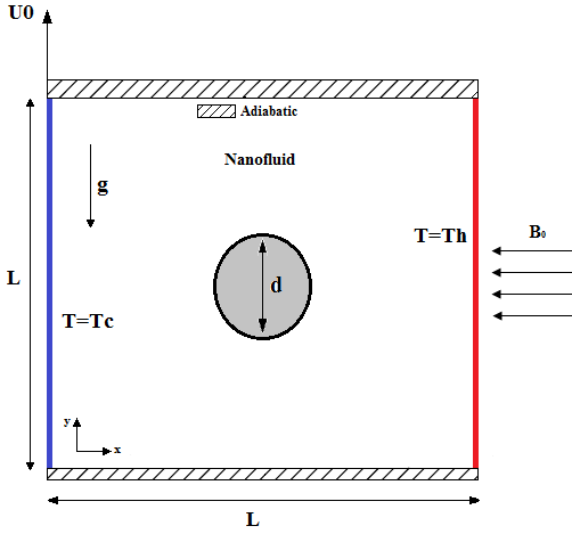

Fig. 1. The geometry of the calculation domain.

2.1. Governing equations

The non-isothermal two-dimensional flow of the nanofluid [29], inside the cavity, is governed by the equations of continuity, momentum, and energy conservation in the nanofluid media. From Maxwell's field equation of Ohm's law, the momentum equation is modified to highlight the Lorentz force [30]. However, the equations of continuity and energy balance remain unchanged. In addition, the properties of the fluid are also assumed constant, except for the density in the buoyancy term, which follows Boussinesq's approximation, the gravitational acceleration acts in the negative vertical direction. Thus, in the Cartesian coordinate system, the basic equations that govern the studied phenomenon are:

Continuity equation:

$$\frac{\partial u}{\partial x}+\frac{\partial v}{\partial y}=0 \qquad 1$$

Momentum equations [29-31]:

$$\rho_{\mathrm{nf}}\left(\frac{\partial u}{\partial t}+u\frac{\partial u}{\partial x}+v\frac{\partial u}{\partial y}\right)=-\frac{\partial p}{\partial x}+\mu_{\mathrm{nf}}\left(\frac{\partial^2 u}{\partial x^2}+\frac{\partial^2 u}{\partial y^2}\right) \qquad 2$$

$$\rho_{\mathrm{nf}}\left(\frac{\partial v}{\partial t}+u\frac{\partial v}{\partial x}+v\frac{\partial v}{\partial y}\right)=-\frac{\partial p}{\partial y}+\mu_{\mathrm{nf}}\left(\frac{\partial^2 v}{\partial x^2}+\frac{\partial^2 v}{\partial y^2}\right)+\rho_{\mathrm{nf}}g\beta_{\mathrm{nf}}\left(T-T_c\right)-B_0^2\sigma_{\mathrm{nf}}v \qquad 3$$

Energy conservation equation:

$$\frac{\partial T}{\partial t}+u\frac{\partial T}{\partial x}+v\frac{\partial T}{\partial y}=\alpha_{\mathrm{nf}}\left(\frac{\partial^2 T}{\partial x^2}+\frac{\partial^2 T}{\partial y^2}\right) \qquad 4$$

Energy conservation equation in the solid part [1]:

$$\frac{\partial T_s}{\partial t}=\alpha_{\mathrm{s}}\left(\frac{\partial^2 T_s}{\partial x^2}+\frac{\partial^2 T_s}{\partial y^2}\right) \qquad 5$$

The stream function ψ [1]is calculated from the velocity field components as follows:

$$\frac{\partial \psi}{\partial x}=-v \text{ and } \frac{\partial \psi}{\partial y}=u \qquad 6$$

Determination of the stream function amounts to solving the following Poisson equation:

$$\frac{\partial^2 \psi}{\partial x^2}+\frac{\partial^2 \psi}{\partial y^2}=\frac{\partial^2 u}{\partial y^2}-\frac{\partial^2 v}{\partial x^2} \qquad 7$$

The dimensionless variables used to generalize the governing balances are defined as follows:

$$X,Y=\frac{x,y}{L}\,,U,V=\frac{u,v}{U_0}\,,P=\frac{p}{\rho_{\mathrm{nf}}U_0^2}\,,\ \theta=\frac{T-T_c}{T_h-T_c}\,,\theta_s=\frac{T_s-T_c}{T_h-T_c}$$

$$and\ \Psi=U_0L\psi \qquad 8$$

Taking into account the above-mentioned assumptions, thenon-dimensional governing equations are as follows:

Dimensionless continuity equation:

$$\frac{\partial U}{\partial X}+\frac{\partial V}{\partial Y}=0 \qquad 9$$

Dimensionless momentum equations:

$$\frac{\partial U}{\partial \tau}+U\frac{\partial U}{\partial X}+V\frac{\partial U}{\partial Y}=-\frac{\partial P}{\partial X}+\frac{\rho_{\mathrm{f}}}{\rho_{\mathrm{nf}}}\frac{\mu_{\mathrm{nf}}}{\mu_{\mathrm{f}}}\frac{1}{\mathrm{Re}}\left(\frac{\partial^2U}{\partial X^2}+\frac{\partial^2U}{\partial Y^2}\right) \qquad 10$$

$$\frac{\partial V}{\partial \tau}+U\frac{\partial V}{\partial X}+V\frac{\partial V}{\partial Y}=-\frac{\partial P}{\partial Y}+\frac{\rho_{\mathrm{f}}}{\rho_{\mathrm{nf}}}\frac{\mu_{\mathrm{nf}}}{\mu_{\mathrm{f}}}\frac{1}{\mathrm{Re}}\left(\frac{\partial^2V}{\partial X^2}+\frac{\partial^2V}{\partial Y^2}\right)+\frac{(\rho\beta)_{\mathrm{nf}}}{\rho_{\mathrm{nf}}\beta_{\mathrm{f}}}\mathrm{Ri}\theta$$

$$-\frac{\rho_{\mathrm{f}}}{\rho_{\mathrm{nf}}}\frac{\sigma_{\mathrm{nf}}}{\sigma_{\mathrm{f}}}\frac{\mathrm{Ha}^2}{\mathrm{Re}}V \qquad 11$$

Dimensionless energy conservation equation:

$$\frac{\partial \theta}{\partial \tau}+U\frac{\partial \theta}{\partial X}+V\frac{\partial \theta}{\partial Y}=\frac{\alpha_{\mathrm{nf}}}{\alpha_{\mathrm{f}}}\frac{1}{\mathrm{Re}\,\mathrm{Pr}}\left(\frac{\partial^2\theta}{\partial X^2}+\frac{\partial^2\theta}{\partial Y^2}\right) \qquad 12$$

The dimensionless energy conservation equation in the solid part:

$$\frac{\partial \theta_{\mathrm{s}}}{\partial \tau}=\frac{\alpha_{\mathrm{s}}}{U_0L}\left(\frac{\partial^2\theta_{\mathrm{s}}}{\partial X^2}+\frac{\partial^2\theta_{\mathrm{s}}}{\partial Y^2}\right) \qquad 13$$

The dimensionless stream functionΨ is calculated by:

$$\frac{\partial \Psi}{\partial X}=-V \text{ and } \frac{\partial \Psi}{\partial Y}=U \qquad 14$$

Dimensionless Poisson equation

$$\frac{\partial^2\Psi}{\partial X^2}+\frac{\partial^2\Psi}{\partial Y^2}=\frac{\partial^2U}{\partial Y^2}-\frac{\partial^2V}{\partial X^2} \qquad 15$$

The physical properties of the nanofluid including density, dynamic viscosity [21], specific heat, thermal conductivity [20], thermal expansion, and electrical conductivity are respectively calculated by:

$$\rho_{nf} = (1-\varphi)\rho_f + \varphi\rho_p \quad 16$$

$$\mu_{nf} = \frac{\mu_f}{(1-\varphi)^{2.5}} \quad 17$$

$$(\rho c_p)_{nf} = (1-\varphi)(\rho c_p)_f + \varphi(\rho c_p)_p \quad 18$$

$$\frac{k_{nf}}{k_f} = \frac{k_p + 2k_f - 2\varphi(k_f - k_p)}{k_p + 2k_f + \varphi(k_f - k_p)} \quad 19$$

$$(\rho\beta)_{nf} = (1-\varphi)(\rho\beta)_f + \varphi(\rho\beta)_p \quad 20$$

$$\sigma_{nf} = (1-\varphi)\sigma_f + \varphi\sigma_p \quad 21$$

The thermal diffusivity α is defined by:

$$\alpha = \frac{k}{\rho c_p} \quad 22$$

In the equations(10)-(12), we notice the appearance of some dimensionless numbers which are: the Reynolds, Prandtl, Richardson, and Hartmann numbers. They are respectively defined by :

$$\mathrm{Re} = \frac{\rho_f U_0 L}{\mu_f},\ \mathrm{Pr} = \frac{\mu_f Cp_f}{k_f},\ \mathrm{Ri} = \frac{g\beta_f (T_h - T_c)}{U_0^2} \text{ and } \mathrm{Ha} = \sqrt{\frac{\sigma_f B_0^2 L}{\mu_f}} \quad 23$$

The thermo-physical properties of the nanoparticles and the base fluid used in the present simulation are mentioned in the following table:

Table 1. Physical properties of the base fluid and nanoparticles [22-24].

Physical Properties	Density [kg/m3]	Dynamic viscosity [Pa.s]	Thermal conductivity [W/(m.K)]	Specific heat [J/(kg.K)]	Electrical conductivity [S/m]	Thermal expansion [1/K]
water	997.1	0.001	0.613	4179	0.05	21×10^{-5}
Al_2O_3	3970	-	40	765	1×10^{-10}	0.85×10^{-5}
CuO	6500	-	18	540	2.7×10^{-8}	0.85×10^{-5}
Fe_3O_4	5200	-	6	670	25000	1.18×10^{-5}

2.2. Boundary conditions

The dimensionless physical form of the boundary conditions[1]can be written as follows:

At the left wall : $U = 0$, $V = 1$, $\theta = 0$ *24*

At the right wall *:* $U = 0$, $V = 0$, $\theta = 1$ *25*

On the surface of the solid : $U = 0$, $V = 0$ *26*

At the top and bottom walls *:* $U = 0$, $V = 1$, $\partial\theta/\partial N = 0$ *27*

At the interface solide-fluid : $\partial\theta s/\partial N = K\,\partial\theta/\partial N$ *28*

With :$K = kf/ks$.

The average Nusselt number of the considered nanofluidsat the heated wall is calculated by the following expression :

$$\mathrm{Nu} = -\frac{k_{\mathrm{nf}}}{k_{\mathrm{f}}} \int_{\text{heated wall}} \frac{\partial\theta}{\partial X}\,\mathrm{d}Y \qquad 29$$

3. Numerical method

3.1. Mesh test

The system of governing equations (9)-(15) with boundary conditions (24)-(28) is solved by using the Galerkin finite element method. The study domain has been discretized with an unstructured triangular mesh. The mesh has been refined near the walls of the cavity and of the obstacle, in order to highlight the flow fluid details. Moreover, in the vicinity of these boundaries, a rectangular layer mesh has been used. The interpolation functions used for discretizing the velocity and temperature are quadratic. However, the pressure is discretized using a linear interpolation function. It should be noted that the convergence criterion of the unknown functions U, V, P, θ, and θ_s relates to the absolute error which must be less than 10^{-6}.

The analysis of the mesh quality and its effect on the numerical results is a fundamental step, for which five meshes have been tested. The elements number, the Nusselt number Nu, the dimensionless temperature θ in the position (X = 0.5, Y = 0.75) of the fluid part and θs in the position (0.5,0.5) of the solid part and the maximum stream function Ψ for each mesh are presented on Table.2. It seems clear that the mesh refinement does not have a significant influence on the results from the second elements number (M2) and it seems that it is not big enough to stabilize the results. From mesh size 4, the expected trend is obtained by appreciating the stabilization of the values of Nu, θs, θ, and Ψ.

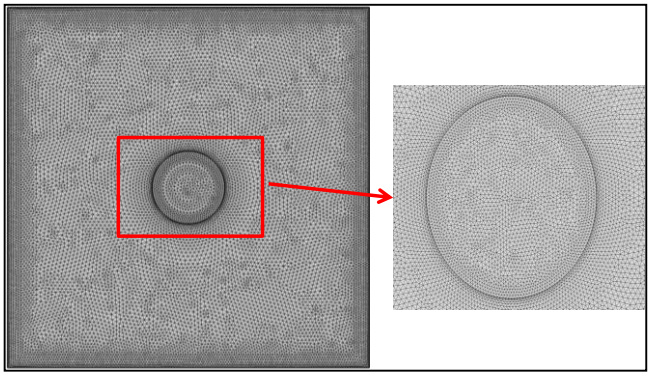

Fig. 2. Typical grid used for simulation.

The convergence time increases systematically with the increase of mesh number. To obtain an acceptable, fairly and accurate solutions, the mesh M4 is privileged to perform the following calculations.

Table 2. Mesh independence test

	elements	Nu	θs	θ	$\lvert\Psi_{max}\rvert$
Mesh 1	2270	3.72758	0.55519	0.73153	0.00991
Mesh 2	5160	3.73286	0.55479	0.73124	0.00996
Mesh 3	8974	3.73465	0.55466	0.73114	0.00997
Mesh 4	14142	3.73509	0.55464	0.73113	0.00998
Mesh 5	20106	3.73508	0.55464	0.73113	0.00998

3.2. Code validation

Figure3 shows a comparison of the results between our numerical work and those of *Rahman et al.* [1]. The isotherms in the cavity for different Richardson numbers are presented with a Hartmann number Ha = 10. We observe a very good concordance between the two results.

Table 3. Comparison of present results with Rahman et al.[1].

Richardson number	Average Nusselt number (Nu)		Deviation %
	Rahman et al. 2010	Present results	
0.0	1.896161	1.907561	0,601
1.0	1.224756	1.226013	0,102
2.0	1.562487	1.562446	0,002
3.0	1.853496	1.851904	0,085
4.0	2.095305	2.092173	0,149
5.0	2.304356	2.299894	0,193

A second comparison with the work of *Rahman et al.*[1] is presented in Table 3, noting that our results obtained from the calculation of the average Nu as a function of the Richardson number are almost identical to those of *Rahman et al.* with a deviation rate that does not exceed 0.6%.

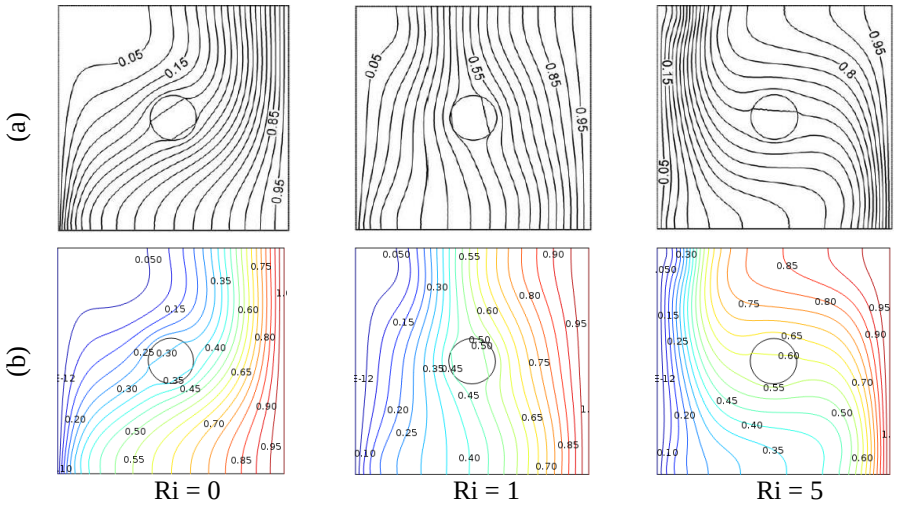

Fig. 3. Isotherms in the cavity for different Richardson numbers, with a Hartmann number Ha = 10 (a) Rahman et al. 2010 (b) present work.

4. Results and discussion

This paper aims to investigate the influence of the nanoparticles' nature on the thermo-magnetohydrodynamic behavior in a square cavity with an obstacle. Representative of streamlines, isotherms, graphs, and tables of average Nusselt number and rate of variation for different value of Hartmann number (Ha = 0-75), volume fraction (φ = 0-0.1), Richardson number (Ri = 0-5), for the three nanoparticles (Al_2O_3, CuO and Fe_3O_4).

4.1. Alumina nanoparticles results

In figure4 we present the isotherms (a) and streamlines (b) of Al_2O_3 for different values of Ha = 0, 25, 50, and 75, with φ = 0.04 and Ri = 3. In Figure.5a, we notice that the increase of the Hartmann number leads to a reorganization of the isotherms, this increase eliminates the buoyancy effect which stabilizes the hot and cold temperature profile. In the solid part, the isotherms show smooth shapes for low values of Ha (0 and 25). As the Hartmann number increases, the effect of the metallic obstacle on the isotherms becomes visible. Indeed, the shape of each isotherm passing through the obstacle refracts in a linear form indicating the presence of the purely conductive heat transfer mode. In addition, the temperature decreases near this zone due to the effect of the Lorentz force which acts in the opposite direction of buoyancy.

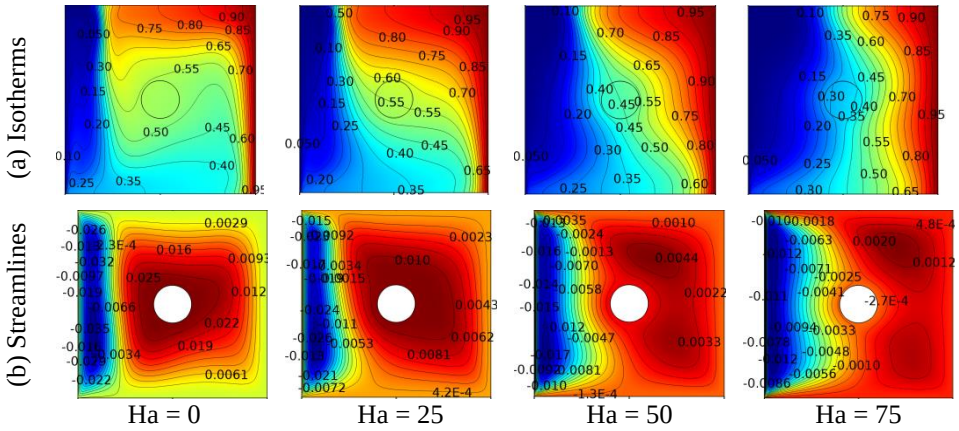

Fig. 4. isotherms (a) and Streamlines(b) for different values of Ha, with Ri = 3, φ = 0.04 and J=0.

Figure 4b represents the variation of the streamlines, we notice that the increase in the Hartmann number favors the vertical stream, we also notice the appearance of secondary vortices for Ha = 50 and 75, there is progressive development of streamlines. On the other hand, the values of the stream function decrease as the Hartmann number increases.

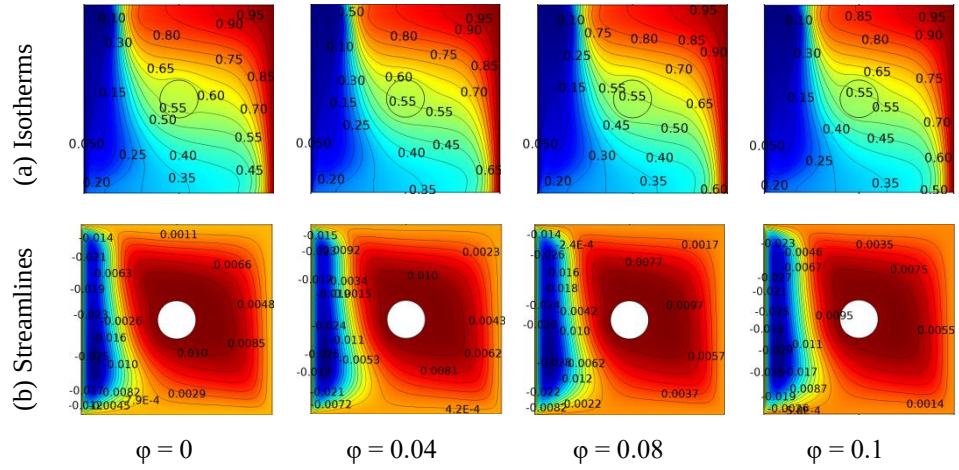

Fig. 5. isotherms (a) and Streamlines(b) for different values of φ,with Ha = 25, Ri =3.

In figure 5a we notice that the isotherms are slightly affected by the increase of the volume fraction. On the other hand, at the level of the obstacle, we observe that the isotherm line is directed upwards, which indicates the cooling of this metallic obstacle. Figure 5b represents the variation of the streamlines, we can see that the increase of the volume fraction does not lead to an important variation of the hydrodynamic structure, however, a relative decrease of the stream function values was observed.

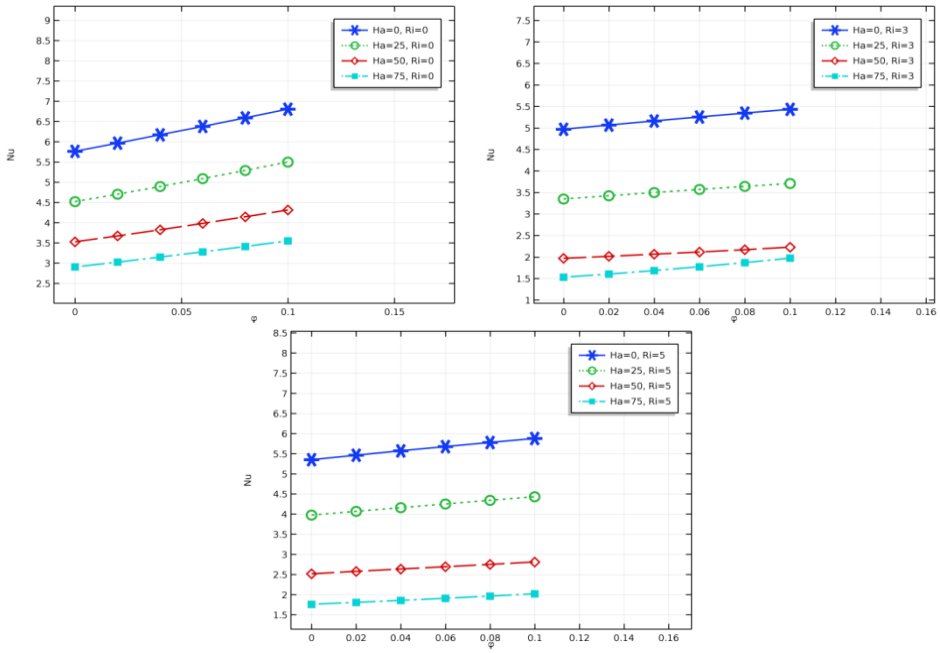

Fig.6. Effect of Ha on average Nusselt Number for different Ha, with J = 0 and Ri = 0,3,5

Figure 6 illustrates the variation of the average Nusselt number (Nu) as a function of the volume fraction for different Ha and Ri. Whatever the values of Ha and Ri the Nu number increases with the increase of the volume fraction of Alumina nanoparticles. Moreover, for all φ and Ha, the values of Nu decrease from Ri = 0 to 3, and then they increase for Ri = 5, which is in agreement with the results obtained by Rahman et al [1].The intensification of the magnetic field induces a significant decrease in the value of the Nusselt number

Table 4. Average Nusselt as a function of volume fraction and Hartmann number for the $Al_2O_3$with : Re = 100, Pr = 0.71, Ri = 3 and J = 0

Volume fraction		0.00	0.02	0.04	0.06	0.08	0.1
Ha = 0	Nu	4.971	5.069	5.165	5.258	5.348	5.436
	%Nu	-	1.971	3.902	5.773	7.583	9.354
Ha = 25	Nu	3.35	3.426	3.501	3.573	3.644	3.712
	%Nu	-	2.268	4.507	6.656	8.776	10.805
Ha = 50	Nu	1.971	2.019	2.068	2.119	2.172	2.23
	%Nu	-	2.435	4.921	7.508	10.197	13.14
Ha = 75	Nu	1.533	1.606	1.686	1.773	1.87	1.976
	%Nu	-	4.761	9.98	15.655	21.983	28.897

Table 4 summarizes the three graphs of the average Nusselt number as a function of volume fraction and Hartmann number for a fixed value of Ri = 3.

The rates of variation of the Nusselt number are also presented in percentage with respect to the base fluid. The convective heat transfer improves and increases with increasing volume fraction and Hartmann number.

4.2. CuO nanoparticles results

the same isotherms and streamlines for CuO are presented in Figures 7a and b for the same conditions. for the isotherms of figure 8a, the increase of the Hartmann number eliminates the buoyancy effect and reorganizes the isotherms which stabilize the hot and cold temperature profile.

This increase makes the effect of the metallic obstacle on the isotherms visible and indicates the presence of the purely conductive mode of heat transfer. On the other hand, the increase in the value of the Hartmann number in figure 7b favors the vertical stream and decreases the values of the stream function, noticing the appearance of secondary vortices for high Hartmann number, thus a progressive development of the streamlines.

We can observe in figure 8a that at the level of the nanofluid, the increase of the volume fraction affects the isotherms slightly. On the contrary, at the level of the obstacle, we notice that the isotherm line goes upwards, which indicates the cooling of this metallic obstacle. This increase in Figure 8b does not cause a significant change in the hydrodynamic structure. However, a relative decrease in the values of the stream function was observed.

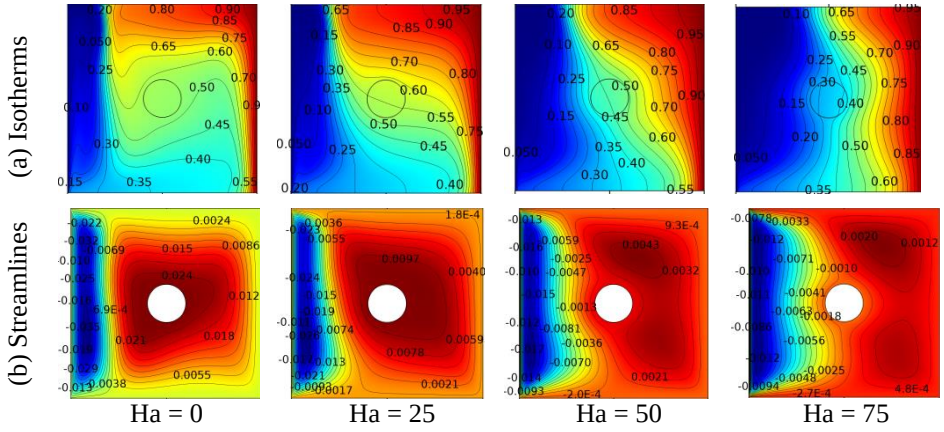

Fig. 7.isotherms (a) and Streamlines(b) for different values of Ha, with Ri = 3, φ = 0.04.

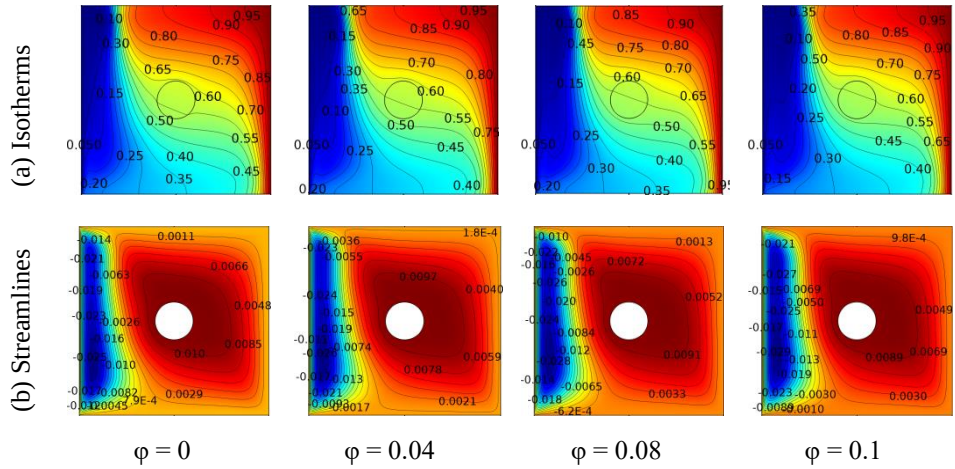

Fig. 8. isotherms (a) and Streamlines(b) for different values of φ,with Ha = 25, Ri =3.

In Figure 9, it is observed that the Nusselt number increases with the increase of the volume fraction of CuO nanoparticles.Moreover, for all values of φ and Ha, Nu decreases from Ri = 0 to Ri = 3 and then they increase for Ri = 5. The intensification of the magnetic field induces a significant decrease in the value of the Nusselt number.

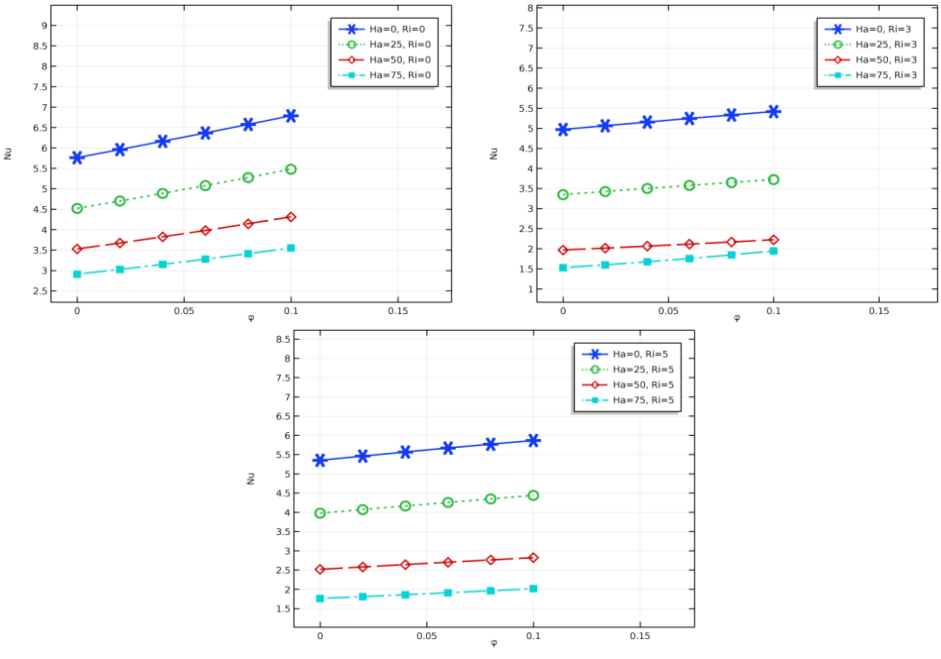

Fig. 9. Effect of Ha on average Nusselt Number for different Ha and Ri = 0, 3, 5.

The three graphs of the average Nusselt value as a function of volume fraction and Hartmann number and the rates of change of the Nusselt number in percentage compared to base fluid the base fluid are summarized in Table 5. we note the improvement and increase in convective heat transfer with the increase in volume fraction and Hartmann number.

We also notice that for the Copper, the rate of change of Nu between Ha=0 and Ha=75 for φ = 0.1 increases by 18.144%.

Table 5. Average Nusselt as a function of volume fraction and Hartmann number for the CuOwith : Re = 100, Pr = 0.71, Ri = 3 and J = 0

Volume fraction		0.00	0.02	0.04	0.06	0.08	0.1
Ha = 0	Nu	4.971	5.066	5.158	5.247	5.334	5.418
	%Nu	-	1.911	3.761	5.552	7.302	8.992
Ha = 25	Nu	3.35	3.428	3.504	3.579	3.653	3.725
	%Nu	-	2.268	4.507	6.656	8.776	10.805
Ha = 50	Nu	1.971	2.019	2.068	2.119	2.172	2.226
	%Nu	-	2.435	4.921	7.508	10.147	12.935
Ha = 75	Nu	1.533	1.606	1.686	1.773	1.87	1.976
	%Nu	-	4.761	9.393	14.807	20.678	27.136

4.3. Fe_3O_4 nanoparticles results

Figure 10a shows the isotherms for different values of Ha for the water-Fe_3O_4 nanofluid, with Ri=3 and φ = 0.04, we remark that the increase of the Hartmann number strongly affects the thermal structure of this ferromagnetic type of nanofluid, due to the importance of the electrical conductivity of the Fe_3O_4 nanoparticles, which is 25000 S/m, eliminating the effect of the thermal buoyancy

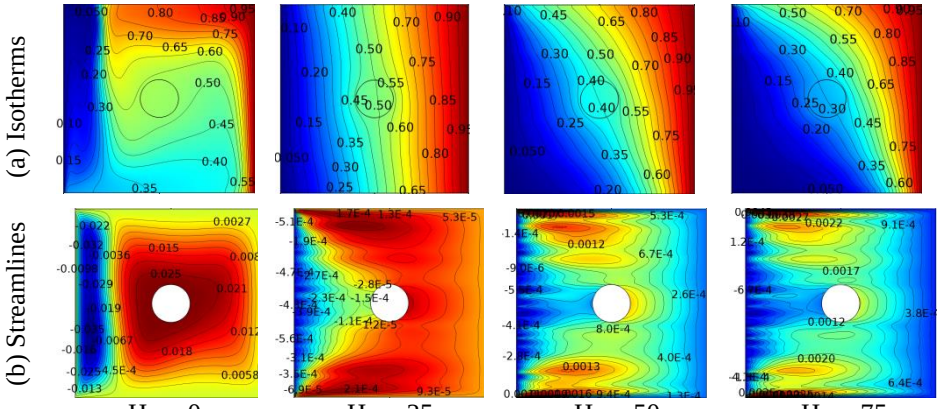

Fig. 10. isotherms (a) and Streamlines(b) for different values of Ha, with Ri = 3, φ = 0.04.

In addition, inside the metallic obstacle, the isotherm curve remains practically smooth as a function of the increase of Ha, which was not observed in the case of the two previous nanofluids, and also the enlargement of the cold zone, especially in the lower part of the cavity.

In Figure 10b, we can see that the hydrodynamic structure of the cavity is destroyed with the existence of several perturbation zones, with a huge reduction of the stream function indicating a quasi immobilization in the laminar flow induced by mixed convection. This favors the conductive heat transfer mode.

Figure 11a presents the isotherms for values of φ varying between 0 and 0.1, for the case of base fluid φ = 0, the thermal profile clearly illustrates the buoyancy phenomenon, however, the addition of a volume concentration of Fe_3O_4 nanoparticles of 0.02 reorganizes horizontally the distribution of isotherms in the cavity. Beyond this concentration, the isotherms tilt in a positive direction of rotation indicating the relative return of the buoyancy effect. Inside the metallic structure, the isothermal lines move towards the hot wall under the effect of the magnetic field with the increase of the volume fraction.

For the streamlines presented in Figure 11b we observe that the hydrodynamic structure of the cavity is absolutely destroyed with the introduction of the least concentration of Fe_3O_4 nanoparticles, the existence of several perturbation zones, with a huge reduction of the stream function indicating a quasi-immobilization in the laminar flow induced by mixed convection. This favors the conductive heat transfer mode.

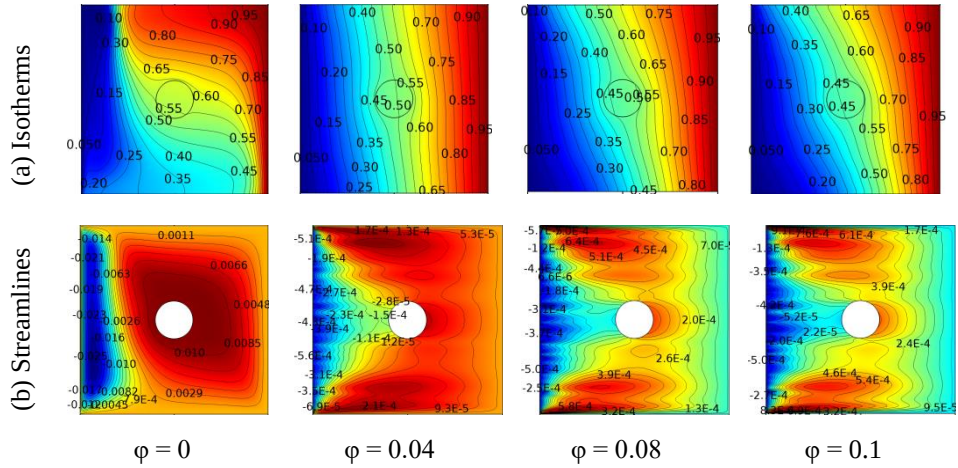

Fig. 11. isotherms (a) and Streamlines(b) for different values of φ,with Ha = 25, Ri =3.

In figure 12, the Nusselt number increases linearly with the volume fraction. In the case of base fluid, the intensification of the magnetic field leads to a remarkable decrease of Nu, however, the introduction of the lower volume fraction in the cases of existence of the magnetic field causes a brutal decrease of the Nusselt number which reaches the value of 1 for Ha = 25 a φ = 0.02. Contrary to the results obtained in the two cases of Alumina and CuO, the number of Nu increases with the increase of Ha (25,50, and 75) and the volume fraction.

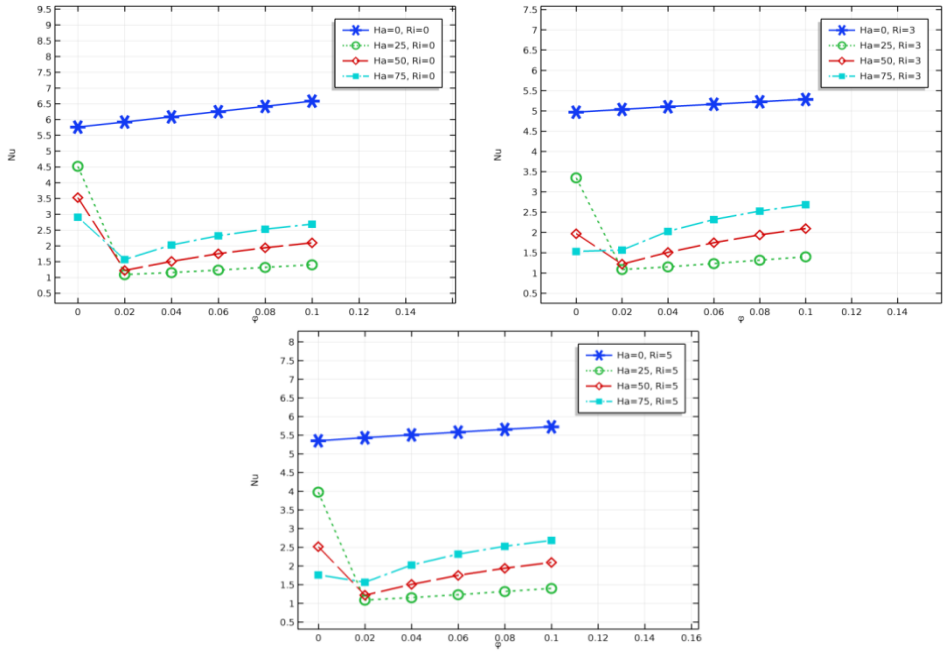

Fig. 12. Effect of φ on average Nusselt Number for different Ha and Ri.

A synthesis of the water-Fe_3O_4 nanofluid is presented in table 6 for the average Nusselt values and its rate of change as a function of φ and Ha for Ri = 3, these rates of change are presented in percentage referencing the base fluid. It can be noticed that the convective heat transfer improves and increases with the increase of the volume fraction and the Hartmann number. It can also be noted that for Fe_3O_4, the rate of change of Nu between Ha=0 and Ha=75 for φ = 0.1 increases by more than 69%.

Table 6. Average Nusselt as a function of volume fraction and Hartmann number for the $Fe_3O_4$with : Re = 100, Pr = 0.71, Ri = 3 and J = 0

Volume fraction		0.00	0.02	0.04	0.06	0.08	0.1
Ha = 0	Nu	4.971	5.039	5.105	5.168	5.228	5.286
	%Nu	-	1.367	2.695	3.962	5.169	6.336
Ha = 25	Nu	3.35	1.088	1.153	1.233	1.318	1.401
	%Nu	-	-67.522	-65.582	-63.194	-60.656	-58.179
Ha = 50	Nu	1.971	1.122	1.51	1.75	1.942	2.098
	%Nu	-	-38.051	-23.389	-11.212	-1.471	6.443
Ha = 75	Nu	1.533	1.567	2.028	2.321	2.529	2.688
	%Nu	-	2.217	32.289	51.404	64.97	75.342

To highlight the difference between the thermal efficiency of the three types of nanoparticles studied, three graphs of Nu of the different nanoparticles in the function of

the volume fraction (φ) have been plotted for different values of Ri (0, 3, and 5) and a Hartmann number Ha = 25.

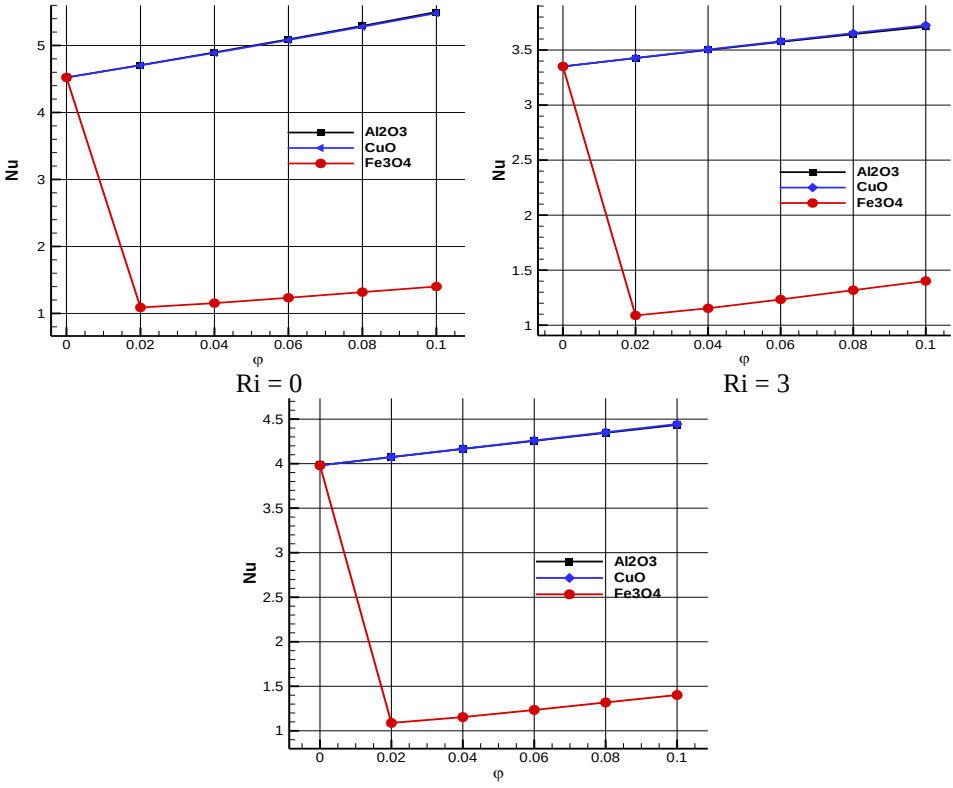

Fig. 13. Variation of the average Nusselt Number for different φ, with Ha = 25 an Ri = 0, 3, 5

Whatever the number of Ri, CuO nanoparticles give a better convective thermal efficiency, while Fe_3O_4 nanoparticles strongly reduce this thermal efficiency, therefore, this type of nanoparticles is deconsecrated for cooling applications of equipment leaking at magnetic field lines.

The results obtained from the numerical simulation of the MHD flow of a nanofluid of three types of nanoparticles (Al_2O_3, CuO, and Fe_3O_4) can be used for the design of cooling systems, such as solar collectors, furnaces, lubrication technologies, drying technologies, and electronic cooling components such as CPU coolers, where the flow is subject to leakage of magnetic field lines from neighboring equipment. In addition, the present results are useful for better understanding practical systems, and for an enriching continuity in the field of nanoparticles, these results can be considered as reference.

5. Conclusion

In this work, a numerical investigation is conducted to determine the effect of Al_2O_3, CuO, and Fe_3O_4 nanoparticles on the thermo-magnetohydrodynamic behavior of a nanofluid in a square cavity equipped with a metallic circular obstacle.

The influence of the Hartmann number and the volume fraction were considered as control parameters of this study. From numerical results obtained, the following points were demonstrated:

- In the case of Al_2O_3 and CuO, the Hartmann number significantly reduces the convective heat transfer in the square cavity with a refraction of the isotherms in the metal part, on the other hand, the transfer rate increases with the increase of non-zero Hartmann number for the case of Fe_3O_4.

- whatever the type of nanoparticle, the volume fraction leads to an increase of the Nusselt number and the cooling of the metallic obstacle.

- the presence of the lowest concentration of iron nanoparticles under the effect of non-zero Hartmann numbers, destroys the hydrodynamic structure within the cavity and causes a quasi immobilization of the laminar flow.

- The CuO nanoparticles give the best heat transfer efficiency by convection, on the other hand, we find a very reduced efficiency for Fe_3O_4.

- The Nusselt number values for CuO and Alumina are very close, which leads us to conclude that Alumina is a better choice for use because of its reduced cost.

This study is suitable to be used for cooling applications, especially for electronic equipment with in-line leakage of magnetic fields. Therefore, iron nanoparticles are not recommended for such equipment.

Nomenclature

Symbols

B_0	Magnetic induction [Wb.m^{-2}]
c_p	Specific heat [J.kg^{-1}.K^{-1}]
g	Gravitational acceleration [m.s^{-2}]
Ha	Hartmann number
k	Thermal conductivity [W.m^{-}1.K^{-1}]
K	Conductivity ratio
L	Cavity length [m]
N	Normal coordinate [m]
Nu	Nusselt number
p	Pressure [N.m^{-2}]
P	Dimensionless pressure
Pr	Prandtl number
Re	Reynolds number
Ri	Richardson number
t	Time [s]
T	Temperature [K]
u, v	Velocity component [m.s^{-1}]
U, V	Dimensionless velocity component
U_0	Vertical wall velocity [m.s^{-1}]
x, y	Cartesian coordinates [m]
X,Y	Dimensionless coordinates

Greek symbols

α	Thermal diffusivity [m^2.s^{-1}]
β	Thermal expansion [K^{-1}]
θ	Dimensionless temperature
μ	Dynamic viscosity [kg.m^{-1}.s^{-1}]
ρ	Density [kg.m^{-3}]
σ	Electrical conductivity [Ω^{-1}.m^{-1}]
τ	Dimensionless time
φ	Volume fraction
ψ	Stream function [m^2.s^{-1}]
Ψ	Dimensionless Stream function

Subscripts

c	Cold
f	Base fluid
h	Hot
nf	Nanofluid
p	Nanoparticles
s	Solid

6. References

[1] M.M. Rahman, M.A. Alim, M.M.A. Sarker: International Communications in Heat and Mass Transfer, 37 (2010) 524–534.

[2] A. H. Mahmoudi, I. Pop, M. Shahi, F. Talebi: Computers & Fluids, 72 (2013) 46–62.

[3] G.C. Bourantas, V.C. Loukopoulos: International Journal of Heat and Mass Transfer, 79 (2014) 930–944.

[4] A. Mahmoudi, I. Mejri, M.A. Abbassi, A. Omri:Powder Technology, 256 (2014) 257–271.

[5] O. Ghaffarpasand: Applied Mathematical Modelling, 40 (2016) 9165–9182.

[6] R. Yousofvand, S. Derakhshan, K. Ghasemi, M. Siavashi: International Journal of Mechanical Sciences, 133 (2017) 73–90.

[7] M. Aghamajidi, M.E.Yazdi, S. Dinarvand, I. Pop: Propulsion and Power Research, 7 (2018) 78–90.

[8] S.E. Ahmed, Z.Z. Rashedc: Case Studies in Thermal Engineering, 14 (2019) 100430.

[9] M.P. Mkhatshwa, S.S. Motsa, M.S. Ayano, P. Sibanda: Case Studies in Thermal Engineering, 18 (2020) 100598.

[10] K. Ghasemi, M. Siavashi: International Journal of Mechanical Sciences, 165 (2020) 105199.

[11] B. Mliki, M.A. Abbassi:Propulsion and Power Research, 10 (2021) 143-154.

[12] F. Bouzit, H. Laidoudi, M. Bouzit.: Defect and Diffusion Forum, 378 (2018)113-124.

[13] B. Mahanthesh, N.S. Shashikumar, B.J. Gireesha, I.L. Animasaun: Journal of Computational Design and Engineering, 6 (2019) 551–561.

[14] B. Mahanthesh, B. J. Gireesha, S.A. Shehzad, N. Ibrar, K. Thriveni: Heat Transfer (2020) 1–17.

[15] I.L. Animasaun, O.K.Koriko, K.S. Adegbie, H.A. Babatunde, R.O. Ibraheem, N. Sandeep, B. Mahanthesh: Journal of Thermal Analysis and Calorimetry (2018). doi.org/10.1007/s10973-018-7379-4.

[16] B.J. Gireesha, B. Mahanthesh, R.S.R. Gorla, P.T. Manjunatha: Heat Mass Transfer, 52(2016) 897–911.

[17] B. Mahanthesh: Mapana Journal of Sciences, 16 (2017) 13-26.

[18] B.J. Gireesha, B. Mahanthesh, K.L. Krupalakshmi: *Results in Physics* (2017), doi.org/10.1016/j.rinp.2017.08.040.

[19] F. Bouzit, H. Laidoudi, B.Blissag, M. Bouzit, A. Ghenaim: Diffusion Foundations Submitted, 16 (2018) 84-95.

[20] J.C. Maxwell, A Treatise on Electricity and Magnetism, vol. II, Oxford University Press, Cambridge, UK, 1873. p. 54.

[21] H.C. Brinkman: J Chem Phys, 20 (1952) 571-581.

[22] S. Hussain, S.E. Ahmedc: Journal of Magnetism and Magnetic Materials, 484 (2019) 356–366.

[23] G.A. Sheikhzadeh, S.Nazari: Transport Phenomena in Nano and Micro Scales, 1 (2013) 138-146.

[24] B. Mliki, M.A.Abbassi, A. Omri, Z. Belkacem: Powder Technology, 308 (2017) 70–83.
[25] A. Mokhefi, M. Bouanini, M. Elmir: International Journal of Heat and Technology, 39 (2021) 251-261.
[26] G.C. Bourantas, V.C. Loukopoulos: International Journal of Heat and Mass Transfer, 79 (2014) 930–944.
[27] A.Mokhefi, M.Bouanini, M.Elmir, P.Spitéri: Metallurgical and Materials Engineering, doi.org/10.30544/626.
[28] I. Mejri , A. Mahmoud , M.A. Abbasi , A. Omri: Powder Technol, 266 (2014) 340–353 .
[29] K.M. Rabbi, M. Sheikholeslami, A. Karim, A. Shafee, Z. Li, I. Tlili:Physica A (2019) doi.org/10.1016/j.physa.2019.123520.
[30] K.R. Cramer, S.I. Pai: Magnetofluid Dynamics for Engineering and Applied Physicists McGraw-Hill, New York, 1974.
[31] A. Mahmoudi: Chinese Journal of Physics, 68 (2020) 618-632.
[32] A.W. Ali , V. Dumitru , F. Constantin: Physics of Fluid, 29 (2017) 082001.
[33] K. Madhura , R. Babitha , S.S.Iyengar: Journal of Nanofluids, 8 (2019) 1158-1169.
[34] M. Narahari , N. Alaparthi , I. Pop: The Canadian Journal of Chemical Engineering, 95 (2017) 1-13.
[35] G. Kalpana , K.R. Madhura , S.S. Iyengar , M.S. Uma: International Journal of Applied and Computational Mathematics, 5 (2019) 5-62.